

A Diffusion Quantum Monte Carlo Approach to the Polaritonic Ground State

Braden M. Weight,^{*,†,‡} Sergei Tretiak,[†] and Yu Zhang^{*,†}

[†]*Department of Physics and Astronomy, University of Rochester, Rochester, NY 14627, U.S.A.*

[‡]*Theoretical Division, Los Alamos National Laboratory, Los Alamos, NM, 87545, U.S.A.*

E-mail: bweight@ur.rochester.edu; zhy@lanl.gov

Abstract

Making and using polaritonic states (i.e., hybrid electron-photon states) for chemical applications have recently become one of the most prominent and active fields that connects the communities of chemistry and quantum optics. Modeling of such polaritonic phenomena using *ab initio* approaches calls for new methodologies, leading to the reinvention of many commonly used electronic structure methods, such as Hartree-Fock, density functional, and coupled cluster theories. In this work, we explore the formally exact diffusion quantum Monte Carlo approach (DQMC) to obtain numerical solutions to the polaritonic ground state during the dissociation of the H₂ molecular system. We examine various electron-nuclear-photon properties throughout the dissociation, such as changes to the minimum of the cavity Born-Oppenheimer surface, the localization of the electronic wavefunction, and the average mode occupation. Finally, we directly compare our results to that obtained with state-of-the-art, yet approximate, polaritonic coupled cluster approaches.

LA-UR-23-28443

Introduction

Recent experimental studies of highly entangled light-matter states, known as polaritons, have been shown their ability to modify chemical reactions^{1–12} and physical properties^{13–19} of both low-^{20–25} and high-dimensional material systems. This has garnered a substantial interest in the theoretical community.^{26–29} Specifically, computational chemists have devoted the past few years toward the “re-generation” of various many-body methods – ubiquitously applied to pristine many-electron systems – for use in the case of strongly correlated electron-photon systems.^{26,28,30} All these approaches attempt to solve a non-relativistic quantum electrodynamical (QED) Hamiltonian for the coupled electron-nuclear-photon system for its eigenstates, usually within the cavity Born-Oppenheimer approximation,^{31–33} being the case for most conventional electronic structure methods. These modified self-consistent (sc) approaches include the scQED Hartree-Fock (scQED-HF),^{32,34} density functional theory (scQED-DFT),^{35–39,39} and coupled cluster theory (scQED-CC) techniques,^{34,40–42} to name a few. Moreover, the analogous methods for excited state simulations have also been recently developed, such as time-dependent scQED-DFT (scQED-TDDFT)^{43–48} and equation of motion scQED-CC (scQED-EOMCCSD).^{42,46,49}

In many of these cases, the drawbacks of the original method are exacerbated in its scQED analogue. For example, to describe the

electron-photon correlations in DFT approach, new exchange-correlation functionals needs to be constructed to explicitly account for such effects.^{35,36,39,50–52} The early attempts at developing such functionals resulted in a dramatic reduction in the quality of treatment of bare electron-electron correlations.^{33,40,41,47,48} While efforts toward constructing improved functionals for the scQED-DFT approach are on-going with marked success,^{51,52} the “exact” effects of the cavity presence on the electronic subsystem, are only trustworthy up to the choice of electron-photon and electron-electron exchange-correlation functionals.

One promising approach is the scQED-CC method, which adds correlation on top of the scQED-HF approach. Here the electron-electron correlations are treated by including single and double excitations, which is known to provide accurate results, even for highly correlated many-electron systems. In fact, the CCSD approach is exact for two-electron systems in the absence of the cavity since the single and double excitations comprise the full configuration interaction limit (up to the choice of basis set). This is no longer valid when the cavity is present, since the cavity photons can be excited to an arbitrary level due to their bosonic nature.⁴⁹ Due to the large computational expense, the scQED-CC method has only been used for small molecular systems coupled to the cavity with typically one or two photonic excitations included. This approach is expected to provide reliable results, even for large light-matter coupling strengths.^{34,41} However, such truncation of the photonic excitations has been shown to contradict the full configuration interaction limit in the strong coupling regimes for simple Hubbard model systems, even when using up to 10 photonic excitations.⁴⁹ Notably, this high-level photonic treatment is usually numerically intractable for models describing realistic molecular systems.

In this work, we explore the polaritonic ground state of the H₂ molecular system coupled to a single quantized cavity mode. We solve the Pauli-Fierz QED Hamiltonian in the long-wavelength approximation using the diffusion quantum Monte Carlo (DQMC) approach. This methodology is formally exact for the two-electron H₂ molecular system, even when many quantized photonic modes are considered. We then directly compare with state-of-the-art polaritonic coupled cluster methods to highlight the inherent approximations in such schemes. Various properties are examined,

such as the localization of the electronic wavefunction and changes to the polaritonic potential energy surface. We also explore a decomposition of the photonic wavefunctions into the number (or Fock) basis. This analysis highlights the discrepancy between the scQED-CCSD and DQMC results due to the inclusion of high-level photonic excitations present even in the ground state. Finally, we examine the average photon number as a function of the nuclear separation length. Our results suggest the DQMC scheme as another chemically relevant approach toward modeling molecular and material systems inside the cavity.

Methodology

Electronic Hamiltonian

The molecular Hamiltonian,

$$\hat{H}_M = \hat{T}_N + \hat{T}_{el} + \hat{V} = \hat{T}_N + \hat{H}_{el}, \quad (1)$$

consists of the nuclear kinetic energy, \hat{T}_N , the electronic kinetic energy, \hat{T}_{el} , and all pairwise Coulomb interactions, $\hat{V} = \hat{V}_{ee} + \hat{V}_{eN} + \hat{V}_{NN}$, between electrons e and nuclei N . The electronic Hamiltonian, $\hat{H}_{el} = \hat{H}_M - \hat{T}_N$, which is approximately solved by many electronic structure software, can be written as an eigenvalue problem and yields the Born-Oppenheimer approximation for the electronic states parameterized by the nuclear positions,

$$\hat{H}_{el}|\psi_j\rangle = E_j|\psi_j\rangle. \quad (2)$$

In this work, we consider a “simple” two-electron H₂ molecular system and its interatomic dissociation inside and outside a photonic cavity. In this case, the electronic Hamiltonian takes the form,

$$\begin{aligned} \hat{H}_{el} = & \frac{\hat{\mathbf{p}}_1^2}{2} + \frac{\hat{\mathbf{p}}_2^2}{2} + \frac{1}{|\hat{\mathbf{r}}_1 - \hat{\mathbf{r}}_2|} - \frac{1}{|\hat{\mathbf{r}}_1 - \mathbf{R}_1|} - \frac{1}{|\hat{\mathbf{r}}_1 - \mathbf{R}_2|} \\ & - \frac{1}{|\hat{\mathbf{r}}_2 - \mathbf{R}_1|} - \frac{1}{|\hat{\mathbf{r}}_2 - \mathbf{R}_2|} + \frac{1}{|\mathbf{R}_1 - \mathbf{R}_2|}, \end{aligned} \quad (3)$$

where $\{\mathbf{R}_1, \mathbf{R}_2\}$ denote the nuclear coordinates, $\{\hat{\mathbf{r}}_1, \hat{\mathbf{r}}_2\}$ and $\{\hat{\mathbf{p}}_1, \hat{\mathbf{p}}_2\}$ are the position and momenta operators of the electrons, respectively. Solving Eq. 2 yields the electronic adiabatic states $|\psi_j\rangle$, their respective eigenenergies E_j , and all subsequent properties. Achieving exact solution has proven to be challenging, even for the state-of-the-art approximate many-body methods, such as density functional theory (DFT). Exact diagonal-

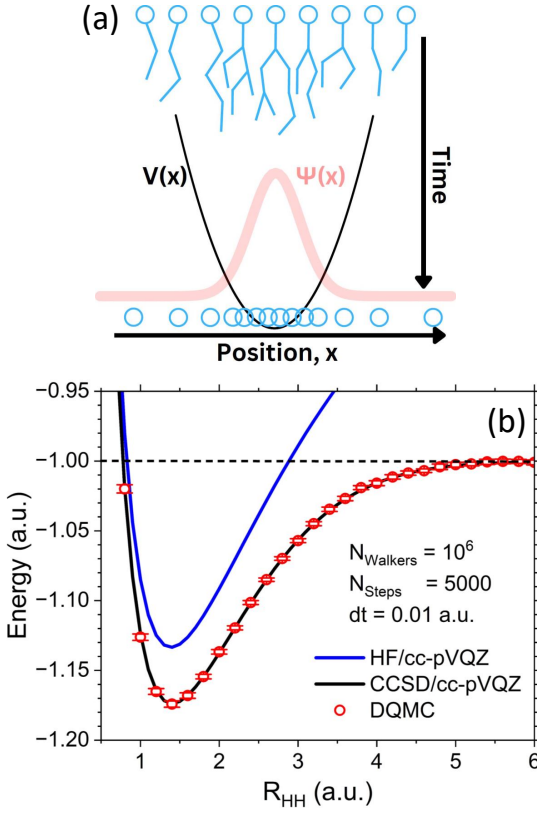


Figure 1: (a) A schematic of the diffusion Monte Carlo process. Gaussian random walkers are initially sampled from a uniform distribution (top blue circles) and move in time (top-to-bottom) by a Gaussian random walk. At each step, the random walker may be removed or duplicated according to the potential energy landscape. (b) The ground state potential energy surface of the H₂ dissociation outside the cavity at various computational levels: Hartree-Fock (HF, blue curve), coupled cluster singles doubles (CCSD, black curve), and diffusion quantum Monte Carlo (DQMC, red circles). Each simulation utilized initial 5000 timesteps to reach equilibrium followed by another 5000 timesteps with $d\tau = 0.01$ a.u. Red error bars represent the standard deviation of the mean energy for each simulation at a fixed nuclear separation length. The horizontal dashed black line indicates the exact dissociation energy of $E_{\text{Diss.}} = -1.0$ a.u.

ization of this Hamiltonian requires the solution of a six-dimensional Hilbert space and can be accomplished via coupled cluster singles and doubles (CCSD), which coincides with the full configuration interaction (FCI) limit for this two-electron system.

Diffusion Monte Carlo

In many cases, the approximate solution to a high-dimensional integral problem can be achieved us-

ing a Monte Carlo approach, which leverages the concept of random variables in a high-dimensional space. Monte Carlo integration is ubiquitous in the community for both classical and quantum mechanical problems, when the number of degrees of freedom (DOFs) is large. One of the most common approaches is Markov-Chain Monte Carlo based on the Metropolis-Hastings algorithm,⁵³ which is related to the variational quantum Monte Carlo (VQMC),⁵⁴ and is used to solve for the equilibrium distribution of the many-particle system.

In this work, we focus on a particular quantum mechanical analogue called diffusion quantum Monte Carlo (DQMC).^{55–61} In DQMC, the wavefunction is approximated by a basis of Gaussian random walkers whose ‘motion’ is defined by multiple applications of a short-time Green’s function for the Schrodinger equation in imaginary time.

The imaginary time Schrodinger equation, in the six-dimensional real-space basis, can be written as,

$$\frac{\partial}{\partial \tau} \psi(\mathbf{r}, \tau) = \left(\frac{1}{2} \nabla_{\mathbf{r}}^2 + V(\mathbf{r}) \right) \psi(\mathbf{r}, \tau), \quad (4)$$

where $\tau = it$ and $\frac{1}{2} \nabla_{\mathbf{r}}^2 = \frac{1}{2} \nabla_{\mathbf{r}_1}^2 + \frac{1}{2} \nabla_{\mathbf{r}_2}^2$. Specifically, $\mathbf{r} = (\mathbf{r}_1, \mathbf{r}_2)$ is a single point in the six-dimensional configuration space of the two electrons in H₂. The formal solution of this equation can be written as a Green’s function,

$$\psi(\mathbf{r}, \tau) = \int d\mathbf{r}' G(\mathbf{r}, \mathbf{r}', \tau) \psi(\mathbf{r}', 0), \quad (5)$$

This propagator $G(\mathbf{r}, \mathbf{r}', \tau)$ can be approximated by the Trotter-Suzuki splitting of the time-evolution operator as^{62,63}

$$e^{(\frac{1}{2} \nabla_{\mathbf{r}}^2 + V(\mathbf{r}))d\tau} \approx e^{\frac{1}{2} \nabla_{\mathbf{r}}^2 d\tau} e^{V(\mathbf{r})d\tau} \quad (6)$$

during a short-time interval $d\tau = \frac{\tau}{N_{\text{steps}}}$ leading to the following Green’s function approach,

$$G(\mathbf{r}, \mathbf{r}', \tau) = \lim_{d\tau \rightarrow 0} \left[G_{\text{Diff.}}(\mathbf{r}, \mathbf{r}', d\tau) G_{\text{Birth/Death}}(\mathbf{r}, \mathbf{r}', d\tau) \right]^{N_{\text{steps}}}. \quad (7)$$

The formal solutions to these Green’s functions are

$$G_{\text{Diff.}}(\mathbf{r}, \mathbf{r}', d\tau) = e^{-\frac{(\mathbf{r}-\mathbf{r}')^2}{2d\tau}} \quad (8)$$

$$G_{\text{Birth/Death}}(\mathbf{r}, \mathbf{r}', d\tau) = e^{-d\tau \frac{V(\mathbf{r})+V(\mathbf{r}')}{2}}. \quad (9)$$

Here, and in the equations above, \mathbf{r} and \mathbf{r}' are two system configurations of the $3N_{\text{el}}$ dimensional

space (the nuclear DOFs are fixed), where N_{el} is the number of electrons ($N_{\text{el}} = 2$ in this case). The first Green's function is the solution to the diffusion equation in free space (*i.e.*, $\partial_\tau \psi = \frac{1}{2} \nabla^2 \psi$), which leads to an unbiased Gaussian random walk with a standard deviation $\sqrt{\tau}$.

The second propagator gives rise to an exponential probability of the Gaussian random walker itself, often called the Birth/Death algorithm. This propagator dictates the multiplication or destruction of a walker according to the probability distribution $\mathcal{P}_w \sim G_{\text{Birth/Death}}(\mathbf{r}', \mathbf{r}, \tau)$, given the current $V(\mathbf{r}')$ and previous $V(\mathbf{r})$ total potential energies (for a single configuration of particles) of the system with configurations \mathbf{r}' and \mathbf{r} , respectively. This term gives rise to a variable number of Gaussian random walkers, which can lead to an exponential increase (or decrease), of the number of walkers.

For practical reasons, one introduces an energy shift, E_T in Eq. 2 by replacing the energy eigenvalue E_j with $E_j - E_T$, where E_T is called the trial energy. The trial energy becomes an estimate of the exact ground state energy after sufficient simulation time, $\lim_{\tau \rightarrow \infty} E_T(\tau) \approx E_0$. As such, this parameter is dynamic and can be understood as a solution to a first-order rate equation for the number of Gaussian random walkers N_w ,

$$\begin{aligned} N_w(\tau + d\tau) &= N_w(\tau) e^{-[E_T(\tau) - E_T(\tau + d\tau)]d\tau} = \bar{N}_w \\ \implies E_T(\tau + d\tau) &= E_T(\tau) + \alpha \log \left(\frac{\bar{N}_w}{N_w(\tau)} \right) \end{aligned} \quad (10)$$

where α and \bar{N}_w are parameters. \bar{N}_w is the target number of random walkers (taken to be 10^6 in this work). $N_w(\tau = 0) = \bar{N}_w$ to initiate the simulation. α is a parameter that controls the stiffness of the variation in the number of random walkers. In this work, we choose $\alpha = 0.01$ a.u., which damps the oscillations in the number of walkers while still allowing them to fluctuate according to the birth/death Green's function without encountering numerical issues such as zero or infinite walkers. A schematic representation of the DQMC method is provided in Fig. 1a.

The DQMC scheme is formally exact for all nodeless ground states, which encompasses up to two Fermions (*e.g.*, electrons) and, in principle, an infinite number of Bosons (*e.g.*, photon modes). It is crucial to emphasize that all results presented in this work converge to the exact answer since we restrict our study to no more than two electrons.

This convergence is ensured when a sufficiently small propagation timestep $d\tau$ is chosen and an adequate number of Gaussian random walkers N_w is used. Extensions of this scheme to ground states that have nodes (or phase changes) and to excited states have been well-studied for electronic systems. This augmentation often involves the fixed-node approximation, which necessitates *a priori* knowledge of the wavefunction's nodal structure. This structure is typically derived from a Hartree-Fock Slater determinant or its post-Hartree-Fock counterparts.

Pauli-Fierz Hamiltonian

The coupling between light and molecular DOFs can take many forms. In this work, we examine the interaction between the H_2 molecular system with a single quantized radiation mode (although there is no limit to the number of modes) using the Pauli-Fierz QED Hamiltonian within the Born-Oppenheimer approximation (*i.e.*, neglecting the nuclear kinetic energy $\hat{T}_{\mathbf{R}}$). Mathematically this Pauli-Fierz Hamiltonian can be written as

$$\begin{aligned} \hat{H}_{\text{PF}} = &\hat{H}_{\text{el}} + \omega_c (\hat{a}^\dagger \hat{a} + \frac{1}{2}) + \omega_c A_0 (\hat{\boldsymbol{\mu}} \cdot \hat{\mathbf{e}}) (\hat{a}^\dagger + \hat{a}) \\ &+ \omega_c A_0^2 (\hat{\boldsymbol{\mu}} \cdot \hat{\mathbf{e}})^2, \end{aligned} \quad (11)$$

where the second term represents the bi-linear light-matter coupling term ($\hat{H}_{\text{el-ph}}$), and the third term denotes the dipole self-energy (\hat{H}_{DSE}), DSE. The interactions between light and matter DOFs are controlled by the molecular dipole operator,

$$\hat{\boldsymbol{\mu}}(\hat{\mathbf{r}}) = - \sum_p^{N_{\text{el}}} \hat{\mathbf{r}}_p + \sum_I^{N_{\text{IONS}}} Z_I \mathbf{R}_I, \quad (12)$$

and its square,

$$\hat{\boldsymbol{\mu}}^2(\hat{\mathbf{r}}) = \sum_{p,p'}^{N_{\text{el}}} \hat{\mathbf{r}}_p \hat{\mathbf{r}}_{p'} - 2 \sum_p^{N_{\text{el}}} \sum_I^{N_{\text{IONS}}} Z_I \hat{\mathbf{r}}_p \mathbf{R}_I + \sum_{I,I'}^{N_{\text{IONS}}} Z_I Z_{I'} \mathbf{R}_I \mathbf{R}_{I'}, \quad (13)$$

which encapsulates both one- and two-electron quadrupole-like terms. As will become clear in the next section, we require the light-matter Hamiltonian in the position representation for the cavity photon mode. Consequently, the Pauli-Fierz

Hamiltonian can be rewritten as

$$\hat{H}_{\text{PF}} = \hat{H}_{\text{el}} + \frac{1}{2}\omega_c^2 \hat{q}_c^2 + \sqrt{2\omega_c^3} A_0 \hat{\mu} \hat{q}_c + \omega_c A_0^2 \hat{\mu}^2, \quad (14)$$

where $\hat{q}_c = \sqrt{\frac{1}{2\omega_c}}(\hat{a}^\dagger + \hat{a})$ represents the position operator for the cavity photon.

Polaritonic Diffusion Monte Carlo

While DQMC has been proven to exactly solve the ground state of Bosonic systems, its extension toward entangled Boson-Fermion systems, particularly those arising from the strong coupling of molecular systems to light in optical or plasmonic cavities, remains under-explored. Nevertheless, extending this method to account for one or several quantized cavity or plasmonic modes, is relatively straightforward using a similar approach by decomposing the exact Green's function into multiple short-time propagators for both the electronic and photonic DOFs .

Namely, we start from the imaginary-time Schrödinger equation for the Pauli-Fierz Hamiltonian in the position representation for both the electrons \mathbf{r} and cavity mode q_c ,

$$\begin{aligned} & \frac{\partial}{\partial \tau} \psi(\mathbf{r}, q_c, \tau) \\ &= \left(\frac{\nabla_{\mathbf{r}}^2}{2} + V(\mathbf{r}) + \frac{\nabla_{q_c}^2}{2} + V_{\text{el-ph}}(\mathbf{r}, q_c) + V_{\text{DSE}}(\mathbf{r}) \right) \times \\ & \quad \psi(\mathbf{r}, q_c, \tau), \end{aligned} \quad (15)$$

where \mathbf{r} again signifies all six real-space coordinates of two electrons. The many-body “local” dipole for a specific configuration \mathbf{r} , can be written as

$$\boldsymbol{\mu}(\mathbf{r}) = - \sum_p^{N_{\text{el}}} \mathbf{r}_p + \sum_I^{N_{\text{IONS}}} \mathbf{R}_I, \quad (16)$$

and subsequent one- and two-electron quadrupole is

$$\begin{aligned} \boldsymbol{\mu}^2(\mathbf{r}) &= \sum_{p,p'}^{N_{\text{el}}} \mathbf{r}_p \mathbf{r}_{p'} - 2 \sum_p^{N_{\text{el}}} \sum_I^{N_{\text{IONS}}} Z_I \mathbf{r}_p \mathbf{R}_I \\ &+ \sum_{I,I'}^{N_{\text{IONS}}} Z_I Z_{I'} \mathbf{R}_I \mathbf{R}_{I'}, \end{aligned} \quad (17)$$

where p and p' label electrons and I and I' denote nuclei. It is worth noting that the nuclear charge

Z_I is 1, $N_{\text{IONS}} = 2$, and $N_{\text{el}} = 2$ for the H₂ cavity system.

Utilizing the Trotter expansion, the kinetic energy of the electrons and photon can be split into one short-time Green's function propagator, while the potential terms can be split into another set as

$$e^{(\frac{\nabla_{\mathbf{r}}^2}{2} + V(\mathbf{r}) + \frac{\nabla_{q_c}^2}{2} + V_{\text{el-ph}}(\mathbf{r}, q_c) + V_{\text{DSE}}(\mathbf{r}))d\tau} \quad (18)$$

$$\begin{aligned} &\approx e^{(\frac{\nabla_{\mathbf{r}}^2}{2} + \frac{\nabla_{q_c}^2}{2})d\tau} e^{(V(\mathbf{r}) + V_{\text{el-ph}}(\mathbf{r}, q_c) + V_{\text{DSE}}(\mathbf{r}) - E_T)d\tau} \\ &\approx e^{(\frac{\nabla_{\mathbf{r}}^2}{2} + \frac{\nabla_{q_c}^2}{2})d\tau} e^{(V_{\text{Total}}(\mathbf{r}, q_c) - E_T)} \end{aligned} \quad (19)$$

over a short-time interval $d\tau$. Here, $V_{\text{Total}}(\mathbf{r}, q_c) = V(\mathbf{r}) + V_{\text{el-ph}}(\mathbf{r}, q_c) + V_{\text{DSE}}(\mathbf{r})$ encompasses all the potential terms. We have also integrated the trial energy E_T directly into the above expression. This leads to the following Green's function approach for the coupled electron-photon system,

$$G(\mathbf{r}, q_c, \mathbf{r}', q'_c, \tau) = \quad (20)$$

$$\lim_{d\tau \rightarrow 0} \left[G_{\text{Diff.}}(\mathbf{r}, q_c, \mathbf{r}', q'_c, d\tau) G_{\text{Birth/Death}}(\mathbf{r}, q_c, \mathbf{r}', q'_c, d\tau) \right]^{N_{\text{steps}}}.$$

In this case, the inclusion of the photonic DOF is formally analogous to an additional effective electronic one with a modified configurational potential energy $V(\mathbf{r}) \rightarrow V(\mathbf{r}) + V_{\text{el-ph}}(\mathbf{r}, q_c) + V_{\text{DSE}}(\mathbf{r}) = V_{\text{Total}}(\mathbf{r}, q_c)$ dependent on its position q_c and the configurational electronic dipole $\mu(\mathbf{r})$ as well as its square $\mu^2(\mathbf{r})$.

The formal solutions to these Green's functions are

$$G_{\text{Diff.}}(\mathbf{r}, q_c, \mathbf{r}', q'_c, d\tau) = e^{-\frac{|\mathbf{r}-\mathbf{r}'|^2}{2d\tau}} e^{-\frac{(q_c-q'_c)^2}{2d\tau}} \quad (21)$$

$$G_{\text{Birth/Death}}(\mathbf{r}, q_c, \mathbf{r}', q'_c, d\tau) = e^{-d\tau \left(\frac{V_{\text{Total}}(\mathbf{r}, q_c) - V_{\text{Total}}(\mathbf{r}', q'_c)}{2} - E_T \right)}. \quad (22)$$

Updating the trial energy E_T follows the same procedure as with photon-free propagation (Eq. 10). The coupled electron-photon wavefunction is constructed by binning Gaussian random walkers at each timestep into a set of equally sized histograms (*i.e.*, shared by all timesteps) such that the creation or destruction of walkers does not affect the histogram binning. Normalization is enforced at the end of the simulation.

Computational Details

For clarity, we present a step-by-step breakdown of the proposed algorithm:

1. Generate initiate configurations by uniformly sampling all DOFs (Electronic Array Size: N_w walkers $\times N_{el}$ electrons $\times 3$ dimensions; Photonic Array Size: N_w walkers $\times N_{modes}$) over a wide enough range, taking special case to sample initial configurations well beyond the nuclear distribution.
2. Evaluate the total potential energy of the system for each configuration $V_{\text{Total}}(\mathbf{r}, q_c)$.
3. Displace all walkers by sampling a Gaussian distribution with a standard deviation of $\sqrt{d\tau}$.
4. Evaluate the total potential energy $V_{\text{Total}}(\mathbf{r}, q_c)$ for the updated configurations.
5. Update the trial energy E_T according to Eq. 10.
6. Calculate walker probabilities as:

$$\mathcal{P}_w = \exp \left[-d\tau \left(\frac{V_{\text{Total}}(\mathbf{r}, q_c) + V_{\text{Total}}(\mathbf{r}', q_c')}{2} - E_T \right) \right]. \quad (23)$$

7. For each walker, compare its probability \mathcal{P}_w to a unique uniform random number ξ and perform one of the following actions
 - (a) Kill the walker if $\mathcal{P}_w < \xi$.
 - (b) Retain the walker if $\xi < \mathcal{P}_w < 1$.
 - (c) Clone/duplicate the walker if $\mathcal{P}_w > 1$.
8. Repeat steps 3-5 until the requested number of steps is completed.
9. Repeat steps 2-6 using the final configurations as the initial configurations for the primary or “production” simulation. Save all average energies and accrue configurational histograms (*i.e.*, the wavefunction) during the production simulation.

Unless otherwise noted, all data reported here use $N_w = 10^6$ walkers, $N_{\text{steps}} = 5000$ steps for the equilibration as well as for the production simulations, $N_{el} = 2$ electrons, and $N_{modes} = 1$ cavity mode. We adopt a numerical timestep of $d\tau = 0.01$ a.u. and a population parameter of $\alpha = 0.01$ a.u. Our implementation is publicly available on GitHub: <https://github.com/bradenmweight/QuantumMonteCarlo>.

Results and Discussion

Bare H₂ Dissociation

The dissociation curve of bare H₂ has been a common benchmark for new many-body methods as well as new density functionals for its simultaneous simplicity and complexity. Given the two-electron constitution, the Born-Oppenheimer surface can be computed exactly using CCSD in the complete basis limit. In contrast, approximate methods, such as Hartree-Fock confined to the mean-field level of electron-electron correlation, perform very poorly for the H₂ dissociation. This can be improved using the broken-symmetry solution (*i.e.*, performing an unrestricted self-consistent field Hartree-Fock analog). However, such a solution, while improving the energy landscape of the mean-field solution, fails to capture precise symmetries of the electron orbitals. Hence, the physical nature of the wavefunction still requires further corrections.

From this perspective, CCSD and HF results comprise the best and worst limits of *ab initio* approaches toward the H₂ dissociation, respectively, and will serve as reference for the current diffusion quantum Monte Carlo (DQMC) study. Figure 1b presents the results of the HF, CCSD and DQMC methods for the pristine (*i.e.*, no cavity) H₂ dissociation. The HF and CCSD results are obtained using the PySCF^{64,65} electronic structure package using the cc-pVQZ basis set. For the DQMC results, the standard deviations of the mean energy are shown as vertical error bars for each nuclear separation length.

In this case, we find that the DQMC approach agrees well with the reference CCSD results. In the case of two electrons, CCSD is expected to perform well, contingent solely on the choice of basis set. However, introduction of the cavity photon mode when incorporating polaritons, leads to harsh approximations in the treatment of both bare photonic excitation and coupled excitations. These truncations in the polaritonic CCSD (or scQED-CCSD) have been comprehensively discussed in existing literature.^{26,28,34,40–42,46,49}

Polaritonic Dissociation Curves

Figure 2 presents the primary results of this work: the polaritonic potential energy surfaces of the H₂ dissociation at varied light-matter coupling strengths A_0 (colors) and cavity frequencies ω_c .

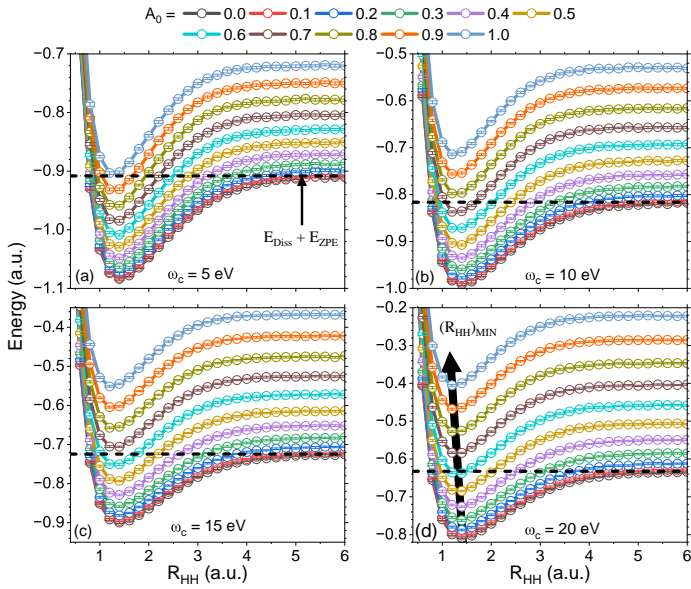


Figure 2: Potential energy surfaces for the ground state H_2 dissociation at various coupling strengths $A_0 = 0.0, 0.1, 0.2, 0.3, 0.4$, and 0.5 a.u. for four cavity frequencies $\omega_c = 5.0$ (a), 10.0 (b), 15.0 (c), and 20.0 (d) eV. Vertical error bars represent the standard deviation of the mean energy. The horizontal dashed line references the expected dissociation energy with vanishing light-matter coupling calculated as $E_{\text{Diss}} + \frac{1}{2}\omega_c$. The cavity polarization is parallel to the bond axis. The black arrow in panel (d) highlights the shift of the minimum energy point $(R_{\text{HH}})_{\text{MIN}}$ in the potential energy surfaces to lower values with increasing light-matter coupling strength A_0 .

For each simulation (*i.e.*, symbol), the standard deviation of the mean energy is shown by a vertical error bar. The horizontal dashed line indicates the expected dissociation energy at zero light-matter coupling , which is computed as the dissociation energy outside the cavity E_{Diss} and the zero-point energy of the cavity mode $E_{\text{ZPE}} = \frac{1}{2}\omega_c$.

Two prominent features can be observed immediately: (I) the vertical energy shift with increasing light-matter coupling strength A_0 and (II) the shift of the minima to lower values of R_{HH} . This first observation is expected, since the primary contribution to the ground state energy is given by the DSE term, which only adds positive values to the total potential energy for each configuration. The second observation is, however, more interesting, since even small changes to such adiabatic surfaces may give rise to a wide range of modified chemistry. For example, the bond stiffness during a chemical reaction, the non-adiabatic couplings between electronic states in photoexcited processes. These phenomena can be monitored by specific

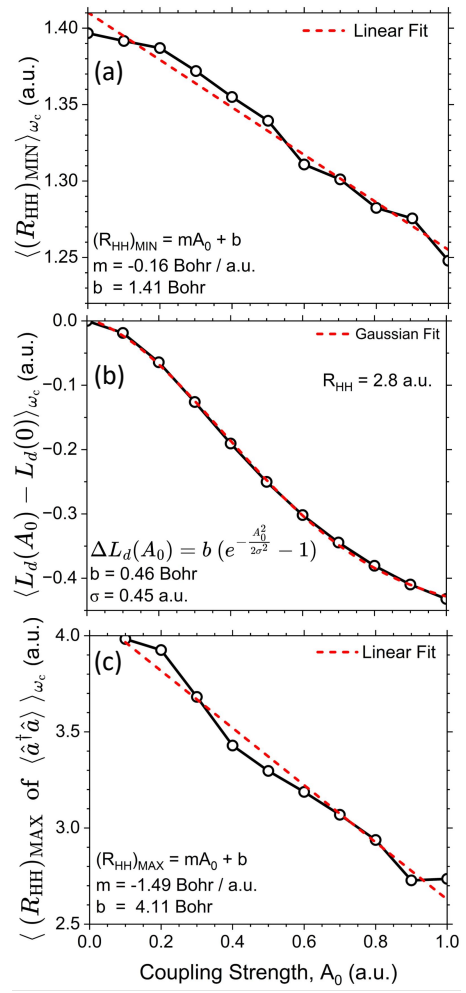


Figure 3: (a) The location of the ground state potential energy surface minimum, (b) the difference in wavefunction localization, and (c) the location of the maximum photon number as function of the light-matter coupling strength A_0 . $\langle \dots \rangle_{\omega_c}$ indicates an average over cavity frequencies $\omega_c = 5.0, 10.0, 15.0$, and 20.0 eV. Panels (a) and (c) are accompanied with a linear fit (red line), and panel (b) is shown with a Gaussian fit (red curve).

spectroscopic signatures, either in the ground (*e.g.*, infrared/Raman) or excited states (*e.g.*, absorption/emission).

The shift of the minimum in the potential energy surface as a function of the light-matter coupling strength A_0 is presented in Fig. 3a. The results are plotted as an average over all four cavity frequencies ($\omega_c = 5.0, 10.0, 15.0$, and 20.0 eV), given the minimal frequency dependency observed. A linear fit to the data shows a slope of $-0.16 \text{ Bohr / a.u.}$ over this range of light-matter coupling A_0 , leading to an overall reduction in nuclear separation of roughly 0.15 Bohr . Even this relatively large amount would result in substantial changes to a

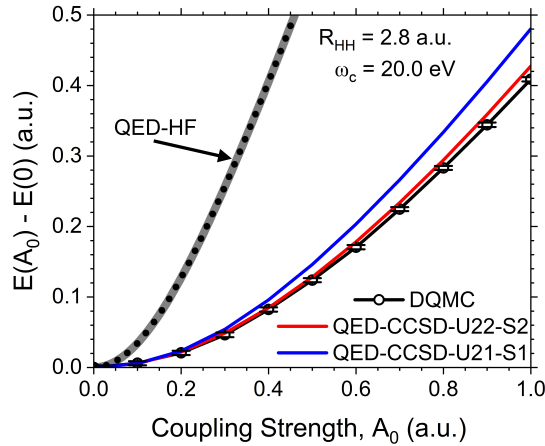


Figure 4: The ground state potential energy of the H_2 system as a function of light-matter coupling strength A_0 . Four methods are compared: DQMC (current work, solid black curve and circles), QED-CCSD-U22-S2 (red curve), QED-CCSD-U21-S1 (blue curve), and QED-HF (dashed black, thick transparent black). The results of the QED-CCSD and QED-HF (thick transparent black) are computed using code published in Ref. 41, and the QED-HF (dashed black) is generated with an in-house code.²⁸ For the DQMC method, since the plot presents the ground state energy with respect to the energy at zero coupling strength, the standard deviation of the difference of the means σ_{A-B} are calculated as $\sigma_{A-B} = \sqrt{\sigma_A^2 + \sigma_B^2}$, where σ_A and σ_B are the standard deviations of the mean for $E(A_0)$ and $E(0)$, The cavity frequency and nuclear separation are fixed at $\omega_c = 20.0$ eV and $R_{\text{HH}} = 2.8$ a.u., respectively.

local chemistry.

At this point, it is prudent to compare/benchmark the results of the DQMC for the polaritonic system with the state-of-the-art coupled cluster approach for polaritonic eigenstates, i.e., the self-consistent QED-CCSD method. This method encompasses diverse treatments of photonic excitation and coupled excitations. In this work, the notation QED-CCSD-U2n-Sm specifies the level of the coupled cluster approach, where n represents the truncation level for the coupled photonic/electronic excitation and m indicates pure photonic excitation. As outlined in Refs. 28,41,66,67, multiple strategies can be applied; we focus on those where $n = m$ and $n \in \{1, 2\}$.

Figure 4 presents the results of these two approaches along with the DQMC of the current work as well as the QED-HF result. The change in the ground state energy, $E(A_0) - E(0)$, of the polaritonic system as a function of the light-matter coupling strength A_0 is shown. The scQED-

CCSD-U21-S1 approach includes only a single photonic excitation and its subsequent interaction with the electronic system. In contrast, the scQED-CCSD-U22-S2 approach includes double excitations of the cavity. This is expected to provide increased accuracy in a similar sense as the double electronic excitations increase the accuracy for the electronic ground state. Firstly, the QED-HF results significantly overestimate the change in ground state energy with increasing light-matter coupling strength. The DQMC approach agrees well with the scQED-CCSD-U22-S2 approach up to roughly $A_0 \sim 0.5$ a.u., beyond which the CCSD results exceed the DQMC's standard deviation. The scQED-CCSD-U21-S1 surpasses the DQMC's error bars around $A_0 \approx 0.2$ a.u. Given that the DQMC method captures exact correlations among electrons and between electrons and photons, we expect that a scQED-CCSD method with increased photonic excitation would align more closely with DQMC energies.

We next inspect the overlaps between the photonic wavefunction and the Fock state basis in the cavity position representation, $c_f(A_0) = \langle \phi_{\text{ph}}^{\text{DQMC}}(A_0) | f \rangle$, where f is the Fock state with f photons and $|\phi_{\text{ph}}^{\text{DQMC}}(A_0)\rangle$ is the wavefunction as computed by the DQMC approach in this study (see Figs. S1, S2 in the **Supporting Information**). At $A_0 = 0.0, 0.5$, and 1.0 a.u., the amplitudes of the zero-photon Fock state are $c_f = 1.0, 0.95$, and 0.89 , respectively. At $A_0 = 1.0$ a.u., there are significant contributions from the higher photon-number Fock states, $c_f : 0.89$ ($f = 0$), 0.37 ($f = 2$), 0.20 ($f = 4$), 0.12 ($f = 6$), and 0.07 ($f = 8$). It is worth noting that contributions from odd-photon-number Fock states are below 0.001, due to the “even”-symmetry of the ground state wavefunction. Furthermore, over 99.5% of the photonic wavefunction is encapsulated by the first 10 Fock states ($0 \leq f \leq 9$) for $A_0 = 1.0$ a.u. This quantitative analysis of the photonic wavefunction underscores the necessity for the scQED-CCSD approach to incorporate additional photonic excitations to capture the required correlations. This also elucidates the discrepancy between the DQMC and scQED-CCSD results at large couplings.

It should be noted that utilizing unperturbed Fock/number states as the basis for photonic DOFs is a user choice. In principle, one may consider a polarized basis, such as the polarized Fock states⁶⁸ or the generalized coherent state basis.⁶⁹ These basis sets introduce a shift in the photonic coordinate

potentially enabling a superior basis to the bare and unshifted Fock states presented in this work. Additionally, by nature of the coupled cluster approach, higher excitation levels than the explicitly included excitation operators are always present due to the exponential anzatz. For example, the authors of Ref. 41 utilized the shifted Fock basis³⁴ in the generation of the scQED-CCSD code used in this work. Thus the results shown in Fig. 4 should benefit from such transformation. Yet, some errors still exist due to the lack of sufficiently large number of photonic excitations.

Here, we have shown that even the state-of-the-art coupled cluster approaches can be far from the exact solution even for simple systems such as H₂. We suggest the DQMC scheme as a valuable tool for gaining insights into elusive correlations within various systems, particularly when testing novel polaritonic many-body techniques.

Returning to the potential energy surface, Figure S4 compares the potential energy surfaces in the cavity to the zero-coupling case, i.e., the differences represented as $E(A_0) - E(0)$. These quantities are shown across a range of light-matter coupling values for four distinct cavity frequencies: (a) 5.0, (b) 10.0, (c) 15.0, and (d) 20.0 eV. A noticeable maximum value emerges, especially in the case of large coupling. This maximum moves to shorter nuclear separation distances, R_{HH} , with increasing light-matter coupling strength. This observation resembles the shift noticed in the minima of the potential energy surface, and it will become apparent in the observables we discuss later in this study. In fact, all of these alterations are closely connected to modifications in the electronic wavefunction, specifically the molecular quadrupole, which is the focus of the upcoming section.

Polaritonic Wavefunctions

Frequently, there is an interest in properties pertaining to the electronic part of the wavefunction confined within the cavity. The alterations noted within the electronic subsystem provide direct information regarding chemical reactions. The photonic wavefunction's expansion in the Fock basis has been previously illustrated in Supplementary Figs. S1, S2. Here we focus on the electronic wavefunction $|\phi_{\text{el}}^{\text{DQMC}}\rangle$ plotted in Fig. 5 at various nuclear separation lengths R_{HH} . For each nuclear separation, the wavefunctions for two distinct coupling strengths, $A_0 = 0.0$ and 0.5 a.u. are shown.

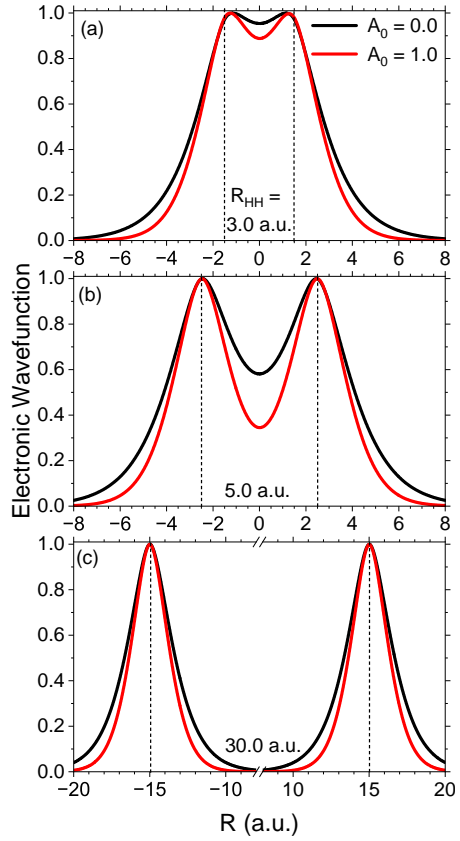


Figure 5: The electronic wavefunction for the H₂ system coupled to the cavity at various nuclear separation lengths $R_{\text{HH}} = 3$ (a), 5 (b), and 30 (c) a.u. for two coupling strengths $A_0 = 0.0$ (black) and 0.5 (red) a.u. The wavefunctions are all normalized by their maximum value for plotting purposes as $\phi_{\text{el}}^{\text{DQMC}} / \text{MAX}[\phi_{\text{el}}^{\text{DQMC}}] \rightarrow \phi_{\text{el}}^{\text{DQMC}}$. For all panels, the cavity frequency is set to $\omega_c = 20.0$ eV with cavity polarization being parallel to the bond axis.

A critical observation pertains to the influence of the cavity on the electronic wavefunction's localization. The underpinning for this behavior can be traced to the Pauli-Fierz Hamiltonian, which incorporates the molecular dipole operator via both direct light-matter interaction $\hat{H}_{\text{el-ph}}$ and through the DSE \hat{H}_{DSE} term in Eq. 11. This implies that the wavefunction tends to become an eigenstate of the dipole (or position) operator, in the limit when $\hat{H}_{\text{el-ph}}, \hat{H}_{\text{DSE}} \gg \hat{H}_{\text{el}}$.

To characterize the localization in quantum mechanical systems, the inverse participation ratio (IPR) is widely used as a quantitative metric.^{70–76} The IPR accesses the spread of a quantum mechanical wavefunction ψ across its basis (in this case,

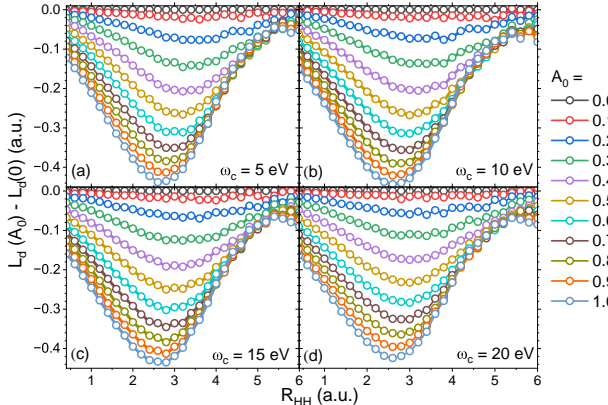


Figure 6: The difference in wavefunction localization of the ground state H_2 dissociation with respect to the pristine system (*i.e.*, no cavity), $L_d(A_0) - L_d(0)$, at various coupling strengths A_0 (colors) for four cavity frequencies $\omega_c = 5.0$ (a), 10.0 (b), 15.0 (c), and 20.0 (d) eV.

real-space position R) and is defined as

$$\text{IPR} = \frac{1}{\sum_j P_j^2}, \quad P_j = \frac{|\psi(R_j)|^2}{\sum_k |\psi(R_k)|^2} \quad (24)$$

Here, $|\psi(R_k)| = \psi(R_k) \equiv \phi_{\text{el}}^{\text{DQMC}}(R_k)$ in this work, since the wavefunction in the position representation is both real- and positive-valued. The resulting IPR spans a range between 1 and N_{basis} , where N_{basis} is the number of basis states (or discrete positions R_j). When $\psi(R_j) = \delta_{R_j, R_0}$, $\text{IPR} = 1$, and when $\psi(R_j) = 1/N_{\text{basis}}$, $\text{IPR} = N_{\text{basis}}$. To convert this value into a spatial length, one can multiply by the grid spacing ΔR to obtain the localization length $L_d = \text{IPR} \times \Delta R$.

Supplementary Figure S3 displays the computed localization length, L_d , for every DQMC simulation of the electronic wavefunction, projected along the bond axis. The most meaningful representation is rather the change in the localization with respect to outside the cavity, $L_d(A_0) - L_d(0)$, which is presented in Fig. 6 for all light-matter coupling strengths A_0 and four cavity frequencies ω_c . There is a pronounced nuclear separation R_{HH} where the localization of the wavefunction exhibits a maximal change compared to outside the cavity, which strongly depends on the light-matter coupling A_0 . This trend mirrors our earlier observations regarding the potential energy surface minimum, as depicted in Fig. 3a. The cavity frequency, again, has minimal effect on the localization of the electronic wavefunction. At a fixed nuclear separation of $R_{\text{HH}} = 2.8$ a.u. (near the maximum localization), the

extent of enhanced wavefunction localization is presented in Fig. 3b and follows a Gaussian function of the coupling strength. The data shown in Fig. 3b represent an average over four cavity frequencies, which provide increased statistical clarity. Our results are suggestive of a generic trend, wherein the electronic localization adheres to a Gaussian profile as a function of the coupling strength. Such Gaussian correlations with coupling strength have also been observed in relation to the splitting between ground and excited state avoided crossings for the LiF system.⁶⁸ These were attributed to a wavefunction overlap between two shifted Fock states (*i.e.*, a Gaussian involving the light-matter coupling strength) in the polarized Fock state representation.

Average Photon Number

The final observable of interest is the average photon number in the ground state. This is a direct extension of our earlier discussion about the overlap of the DQMC photonic wavefunction with the number (or Fock) basis (see Supplementary Fig. S2). In the photon number basis, the expression $\langle \hat{a}^\dagger \hat{a} \rangle$ represents the average occupation of the mode in the Pauli-Fierz (or length) gauge, which may differ from that in the Coulomb (or “ $p \cdot A$ ”) gauge. Nevertheless, the average occupation can undergo a unitary rotation to any other gauge,^{26,77} and we expect that the absolute magnitudes of the photon number might differ, but the physical trends should remain unchanged.

Figure 7a-d presents the average photon number $\langle \hat{a}^\dagger \hat{a} \rangle$ throughout the H_2 dissociation, for various light-matter coupling strengths A_0 and for four cavity frequencies ω_c . Analogous to the previous observables, such as the change in electronic wavefunction localization L_d , there is a distinct peak in photon number at a certain value of R_{HH} , depending on the coupling strength A_0 . The peak’s location is illustrated in Fig. 3c and fit to a linear function, where the data has been averaged over the four cavity frequencies ω_c .

At a fixed $R_{\text{HH}} = 2.8$ a.u., as depicted in Fig. 7e, the average photon number behaves intriguingly. For smaller light-matter coupling strengths $A_0 \leq 0.5$ a.u., the photon number increases quadratically, $\langle \hat{a}^\dagger \hat{a} \rangle \sim \omega_c A_0^2$, with its leading coefficient dependent on the cavity frequency. Conversely, for larger light-matter coupling $A_0 \geq 0.5$ a.u., the average photon number increases linearly (up to the

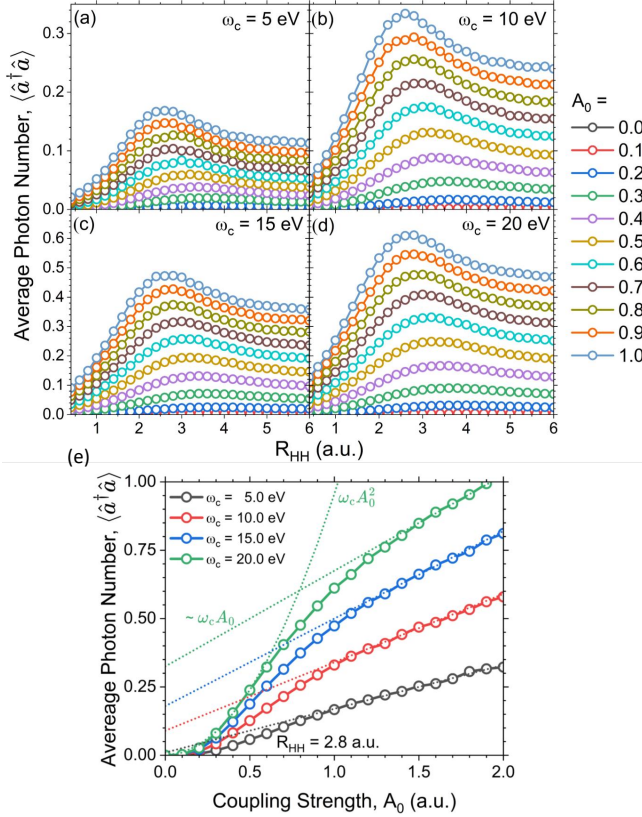


Figure 7: The average photon number, $\langle \hat{a}^\dagger \hat{a} \rangle$, throughout the ground state H_2 dissociation with respect to the uncoupled system, $L_d(A_0) - L_d(0)$, at various coupling strengths A_0 (colors) for four cavity frequencies $\omega_c = 5.0$ (a), 10.0 (b), 15.0 (c), and 20.0 (d) eV. (e) The average photon number, $\langle \hat{a}^\dagger \hat{a} \rangle$, as a function of light-matter coupling strength A_0 for a fixed nuclear separation $R_{\text{HH}} = 2.8$ a.u. for four cavity frequencies $\omega_c = 5.0$ (black), 10.0 (red), 15.0 (blue), and 20.0 (green) eV. The dotted curves present the scaling at the low (*i.e.*, quadratic) and high (*i.e.*, linear) coupling regimes.

maximal coupling strength computed in this work with slopes dependent of the cavity frequency, $\langle \hat{a}^\dagger \hat{a} \rangle \sim \omega_c A_0$. The convergence of the average photon number in the ground state is tested with respect to simulation timestep, as shown in Supplementary Fig. S5. Given these substantial changes in the photon number, there exists potential for fascinating quantum measurements in highly entangled many-body states, especially in dynamic scenarios where complex interplay between the nuclear and photonic DOFs can induce significant fluctuations in the photon number, even in the ground polaritonic state.

Conclusions

In summary, this work presents a diffusion quantum Monte Carlo (DQMC) scheme for direct simulations of molecular polaritons, which necessarily includes complicated correlations between the electronic, nuclear, and photonic degrees of freedom. This scheme represents a thoroughly *ab initio* approach, which is formally exact for the two-electron system interacting with, in principle, infinite cavity modes. As a testament to its capabilities, we study the H_2 molecular dissociation coupled to a single cavity mode. The results are compared directly with state-of-the-art quantum electrodynamical (QED) coupled cluster approaches, which is a formally exact solution to the pristine molecular system (in the absence of cavity). We emphasize that the accuracy of the latter method is largely contingent upon the truncation of photonic excitation in the exponential ansatz. Our comparative analysis evidence that even the highest fidelity approach currently available fails in even the simplest molecular system when the light-matter coupling strengths become large enough to necessarily include contributions from photonic excitations beyond one or two photonic number (or Fock) states.

The DQMC approach is then used to explore various observables for the H_2 system, such as the localization extent of the electronic and the decomposition of the photonic wavefunctions in the Fock basis. Additionally, linear trends in the light-matter coupling strength are identified for the nuclear separations which exhibit (I) the minimum of the potential energy surfaces and (II) the maximum average photon number. Moreover, a Gaussian trend emerges in the changes related to wavefunction localization. In the former two cases, the change of the properties with respect to the nuclear separation length are directly relevant to modifications of chemical reactions, where even the smallest nuclear displacement may alter reaction pathways and resulting products. Meanwhile, the wavefunction's localization can offer insights into processes demanding wavefunction overlap, such as Dexter energy transfer or H/J-aggregates (interacting excitonic systems). This holds implications for exciton-polariton transport in molecular and solid-state materials.

Altogether DQMC represents a promising route toward the direct and accurate simulation of simple systems, where the results are exact. Applications to more intricate systems are possible as

well by leveraging the fixed node approximation for many-electron systems and excited states.^{54,78–80} We note that in the realm of polaritonic DQMC, the fixed node approximation needs to be carefully implemented, since the nodal surface will likely undergo changes as a result of interaction with the cavity. Thus, using a mean-field wavefunction (*i.e.*, Hartree-Fock) must either (I) include the cavity effects on the single-particle orbitals (*i.e.*, QED-HF)⁸¹ or (II) allow the nodal surface to relax in order to minimize the energy while retaining the correct electronic statistics. These ideas direct our future studies in this area.

Presented DQMC approach can be further readily employed to explore polaron formation and its inherent properties, including polaron radius and binding energy, given the bosonic nature of both photons and phonons. Most importantly, and without loss of accuracy, the many-molecule and many-cavity-mode systems can be directly simulated, assuming (I) the molecules do not interact directly via Coulomb potential (*i.e.*, only through mutual interaction with the cavity) and (II) the cavity modes do not include the complex-valued nature of the Pauli-Fierz Hamiltonian in the absence of the long-wavelength approximation. Despite these constraints, our approach illuminates solutions for simple molecular systems inside the cavity. Further, the extension toward plasmonic cavities, where the light-matter coupling strength depends on position, $A_0 \rightarrow A_0(\mathbf{r})$, would be straightforward with minimal changes to the code. DQMC's relative simplicity and favorable scaling with dimensionality, typically a constraint for advanced methods like coupled cluster, cements its place as a promising tool for investigating *ab initio* molecular systems inside cavities.

Author Contributions

We strongly encourage authors to include author contributions and recommend using CRediT for standardised contribution descriptions. Please refer to our general author guidelines for more information about authorship.

Conflicts of interest

There are no conflicts to declare.

Acknowledgements

The authors acknowledge the support from the Laboratory Directed Research and Development Funds (LDRD) at Los Alamos National Laboratory (LANL) and the US DOE, Office of Science, Basic Energy Sciences, Chemical Sciences, Geosciences, and Biosciences Division under Triad National Security, LLC (“Triad”) contract Grant 89233218CNA000001 (FWP: LANLECF7). The research is performed in part at the Center for Integrated Nanotechnologies (CINT), a U.S. Department of Energy, Office of Science user facility at LANL. LANL is operated by Triad National Security, LLC, for the National Nuclear Security Administration of the U.S. Department of Energy (Contract No. 89233218CNA000001). Computing resources were provided by the Center for Integrated Research Computing (CIRC) at the University of Rochester.

References

- (1) Nagarajan, K.; Thomas, A.; Ebbesen, T. W. Chemistry under Vibrational Strong Coupling. *J. Am. Chem. Soc.* **2021**, *143*, 16877–16889.
- (2) Garcia-Vidal, F. J.; Ciuti, C.; Ebbesen, T. W. Manipulating matter by strong coupling to vacuum fields. *Science* **2021**, *373*.
- (3) Hutchison, J. A.; Schwartz, T.; Genet, C.; Devaux, E.; Ebbesen, T. W. Modifying Chemical Landscapes by Coupling to Vacuum Fields. *Angew. Chem. Int. Ed.* **2012**, *51*, 1592–1596.
- (4) Schwartz, T.; Hutchison, J. A.; Genet, C.; Ebbesen, T. W. Reversible Switching of Ultrastrong Light-Molecule Coupling. *Phys. Rev. Lett.* **2011**, *106*, 196405.
- (5) Ebbesen, T. W. Hybrid Light–Matter States in a Molecular and Material Science Perspective. *Acc. Chem. Res.* **2016**, *49*, 2403–2412.
- (6) Sau, A.; Nagarajan, K.; Patrahau, B.; Lethuillier-Karl, L.; Vergauwe, R. M. A.; Thomas, A.; Moran, J.; Genet, C.; Ebbesen, T. W. Modifying Woodward–Hoffmann Stereoselectivity Under Vibrational Strong

- Coupling. *Angew. Chem. Int. Ed.* **2021**, *60*, 5712–5717.
- (7) Thomas, A.; Lethuillier-Karl, L.; Nagarajan, K.; Vergauwe, R. M. A.; George, J.; Chervy, T.; Shalabney, A.; Devaux, E.; Genet, C.; Moran, J.; Ebbesen, T. W. Tilting a ground-state reactivity landscape by vibrational strong coupling. *Science* **2019**, *363*, 615–619.
- (8) Thomas, A.; George, J.; Shalabney, A.; Dryzhakov, M.; Varma, S. J.; Moran, J.; Chervy, T.; Zhong, X.; Devaux, E.; Genet, C.; Hutchison, J. A.; Ebbesen, T. W. Ground-State Chemical Reactivity under Vibrational Coupling to the Vacuum Electromagnetic Field. *Angew. Chem. Int. Ed.* **2016**, *55*, 11462–11466.
- (9) Thomas, A.; Jayachandran, A.; Lethuillier-Karl, L.; Vergauwe, R. M. A.; Nagarajan, K.; Devaux, E.; Genet, C.; Moran, J.; Ebbesen, T. W. Ground state chemistry under vibrational strong coupling: dependence of thermodynamic parameters on the Rabi splitting energy. *Nanophotonics* **2020**, *9*, 249–255.
- (10) Lather, J.; Bhatt, P.; Thomas, A.; Ebbesen, T. W.; George, J. Cavity Catalysis by Cooperative Vibrational Strong Coupling of Reactant and Solvent Molecules. *Angew. Chem. Int. Ed.* **2019**, *58*, 10635–10638.
- (11) Hirai, K.; Hutchison, J. A.; Uji-i, H. Molecular Chemistry in Cavity Strong Coupling. *Chem. Rev.* **2023**, *123*, 8099–8126.
- (12) Simpkins, B. S.; Dunkelberger, A. D.; Vurkafman, I. Control, Modulation, and Analytical Descriptions of Vibrational Strong Coupling. *Chemical Reviews* **0**, *0*, null.
- (13) Thomas, A.; Devaux, E.; Nagarajan, K.; Rogez, G.; Seidel, M.; Richard, F.; Genet, C.; Drillon, M.; Ebbesen, T. W. Large Enhancement of Ferromagnetism under a Collective Strong Coupling of YBCO Nanoparticles. *Nano Lett.* **2021**, *21*, 4365–4370.
- (14) Vergauwe, R. M. A.; Thomas, A.; Nagarajan, K.; Shalabney, A.; George, J.; Chervy, T.; Seidel, M.; Devaux, E.; Torbeev, V.; Ebbeisen, T. W. Modification of Enzyme Activity by Vibrational Strong Coupling of Water. *Angew. Chem. Int. Ed.* **2019**, *58*, 15324–15328.
- (15) Berghuis, A. M.; Serpenti, V.; Ramezani, M.; Wang, S.; Rivas, J. G. Light–Matter Coupling Strength Controlled by the Orientation of Organic Crystals in Plasmonic Cavities. *J. Phys. Chem. C* **2020**, *124*, 12030–12038.
- (16) Berghuis, A. M.; Tichauer, R. H.; de Jong, L. M. A.; Sokolovskii, I.; Bai, P.; Ramezani, M.; Murai, S.; Groenhof, G.; Rivas, J. G. Controlling Exciton Propagation in Organic Crystals through Strong Coupling to Plasmonic Nanoparticle Arrays. *ACS Photonics* **2022**, *9*, 2263–2272.
- (17) Xu, D.; Mandal, A.; Baxter, J. M.; Cheng, S.-W.; Lee, I.; Su, H.; Liu, S.; Reichman, D. R.; Delor, M. Ultrafast imaging of polariton propagation and interactions. *Nat Commun* **2023**, *14*, 3881.
- (18) Deng, H.; Haug, H.; Yamamoto, Y. Exciton-polariton Bose-Einstein condensation. *Rev. Mod. Phys.* **2010**, *82*, 1489–1537.
- (19) Rozenman, G. G.; Akulov, K.; Golombek, A.; Schwartz, T. Long-Range Transport of Organic Exciton-Polaritons Revealed by Ultrafast Microscopy. *ACS Photonics* **2018**, *5*, 105–110.
- (20) Lüttgens, J. M.; Berger, F. J.; Zaumseil, J. Population of Exciton–Polaritons via Luminescent sp₃ Defects in Single-Walled Carbon Nanotubes. *ACS Photonics* **2021**, *8*, 182–193.
- (21) Möhl, C.; Graf, A.; Berger, F. J.; Lüttgens, J.; Zakharko, Y.; Lumsargis, V.; Gather, M. C.; Zaumseil, J. Trion-Polariton Formation in Single-Walled Carbon Nanotube Microcavities. *ACS Photonics* **2018**, *5*, 2074–2080.
- (22) Graf, A.; Tropf, L.; Zakharko, Y.; Zaumseil, J.; Gather, M. C. Near-infrared exciton-polaritons in strongly coupled single-walled carbon nanotube microcavities. *Nat Commun* **2016**, *7*, 13078.

- (23) Graf, A.; Held, M.; Zakharko, Y.; Tropf, L.; Gather, M. C.; Zaumseil, J. Electrical pumping and tuning of exciton-polaritons in carbon nanotube microcavities. *Nature Mater.* **2017**, *16*, 911–917.
- (24) Son, M.; Armstrong, Z. T.; Allen, R. T.; Dhavamani, A.; Arnold, M. S.; Zanni, M. T. Energy cascades in donor-acceptor exciton-polaritons observed by ultrafast two-dimensional white-light spectroscopy. *Nat Commun* **2022**, *13*, 7305.
- (25) Allen, R. T.; Dhavamani, A.; Son, M.; Kéna-Cohen, S.; Zanni, M. T.; Arnold, M. S. Population of Subradiant States in Carbon Nanotube Microcavities in the Ultrastrong Light–Matter Coupling Regime. *J. Phys. Chem. C* **2022**, *126*, 8417–8424.
- (26) Mandal, A.; Taylor, M.; Weight, B.; Koessler, E.; Li, X.; Huo, P. Theoretical Advances in Polariton Chemistry and Molecular Cavity Quantum Electrodynamics. **2022**,
- (27) Ruggenthaler, M.; Sidler, D.; Rubio, A. Understanding polaritonic chemistry from ab initio quantum electrodynamics. **2022**,
- (28) Weight, B. M.; Li, X.; Zhang, Y. Theory and modeling of light-matter interactions in chemistry: current and future. 2023; <http://arxiv.org/abs/2303.10111>.
- (29) Wang, D. S.; Yelin, S. F. A Roadmap Toward the Theory of Vibrational Polariton Chemistry. *ACS Photonics* **2021**, *8*, 2818–2826.
- (30) Foley IV, J. J.; McTague, J. F.; DePrince III, A. E. Ab initio methods for polariton chemistry. 2023; <http://arxiv.org/abs/2307.04881>.
- (31) Flick, J.; Appel, H.; Ruggenthaler, M.; Rubio, A. Cavity Born–Oppenheimer Approximation for Correlated Electron–Nuclear–Photon Systems. *J. Chem. Theory Comput.* **2017**, *13*, 1616–1625.
- (32) Schnappinger, T.; Sidler, D.; Ruggenthaler, M.; Rubio, A.; Kowalewski, M. Cavity-Born-Oppenheimer Hartree-Fock Ansatz: Light-matter Properties of Strongly Coupled Molecular Ensembles. 2023; <http://arxiv.org/abs/2307.02208>.
- (33) Weight, B. M.; Krauss, T. D.; Huo, P. Investigating Molecular Exciton Polaritons Using Ab Initio Cavity Quantum Electrodynamics. *J. Phys. Chem. Lett.* **2023**, *14*, 5901–5913.
- (34) Haugland, T. S.; Ronca, E.; Kjønstad, E. F.; Rubio, A.; Koch, H. Coupled Cluster Theory for Molecular Polaritons: Changing Ground and Excited States. *Phys. Rev. X* **2020**, *10*, 041043.
- (35) Flick, J.; Schäfer, C.; Ruggenthaler, M.; Appel, H.; Rubio, A. Ab Initio Optimized Effective Potentials for Real Molecules in Optical Cavities: Photon Contributions to the Molecular Ground State. *ACS Photonics* **2018**, *5*, 992–1005.
- (36) Pellegrini, C.; Flick, J.; Tokatly, I. V.; Appel, H.; Rubio, A. Optimized Effective Potential for Quantum Electrodynamical Time-Dependent Density Functional Theory. *Phys. Rev. Lett.* **2015**, *115*, 093001.
- (37) Flick, J.; Rivera, N.; Narang, P. Strong light-matter coupling in quantum chemistry and quantum photonics. *Nanophotonics* **2018**, *7*, 1479–1501.
- (38) Ruggenthaler, M.; Flick, J.; Pellegrini, C.; Appel, H.; Tokatly, I. V.; Rubio, A. Quantum-electrodynamical density-functional theory: Bridging quantum optics and electronic-structure theory. *Phys. Rev. A* **2014**, *90*, 012508.
- (39) Ruggenthaler, M.; Tancogne-Dejean, N.; Flick, J.; Appel, H.; Rubio, A. From a quantum-electrodynamical light–matter description to novel spectroscopies. *Nat. Rev. Chem.* **2018**, *2*, 1–16.
- (40) Haugland, T. S.; Schäfer, C.; Ronca, E.; Rubio, A.; Koch, H. Intermolecular interactions in optical cavities: An ab initio QED study. *J. Chem. Phys.* **2021**, *154*, 094113.
- (41) Pavošević, F.; Hammes-Schiffer, S.; Rubio, A.; Flick, J. Cavity-Modulated Proton Transfer Reactions. *J. Am. Chem. Soc.* **2022**, *144*, 4995–5002.
- (42) DePrince, A. E. Cavity-modulated ionization potentials and electron affinities from quantum electrodynamics coupled-cluster theory. *J. Chem. Phys.* **2022**, *154*, 094112.

- (43) Flick, J.; Narang, P. Ab initio polaritonic potential-energy surfaces for excited-state nanophotonics and polaritonic chemistry. *J. Chem. Phys.* **2020**, *153*, 094116.
- (44) Yang, J.; Ou, Q.; Pei, Z.; Wang, H.; Weng, B.; Shuai, Z.; Mullen, K.; Shao, Y. Quantum-electrodynamical time-dependent density functional theory within Gaussian atomic basis. *J. Chem. Phys.* **2021**, *155*, 064107.
- (45) Yang, J.; Pei, Z.; Leon, E. C.; Wickizer, C.; Weng, B.; Mao, Y.; Ou, Q.; Shao, Y. Cavity quantum-electrodynamical time-dependent density functional theory within Gaussian atomic basis. II. Analytic energy gradient. *The Journal of Chemical Physics* **2022**, *156*, 124104.
- (46) Liebenthal, M. D.; Vu, N.; DePrince, A. E. Equation-of-motion cavity quantum electrodynamics coupled-cluster theory for electron attachment. *J. Chem. Phys.* **2022**, *156*, 054105.
- (47) Liebenthal, M. D.; Vu, N.; Iii, A. E. D. Mean-Field Cavity Effects in Quantum Electrodynamics Density Functional and Coupled-Cluster Theories.
- (48) Vu, N.; McLeod, G. M.; Hanson, K.; DePrince, A. E. Enhanced Diastereocontrol via Strong Light–Matter Interactions in an Optical Cavity. *J. Phys. Chem. A* **2022**, *126*, 9303–9312.
- (49) Mordovina, U.; Bungey, C.; Appel, H.; Knowles, P. J.; Rubio, A.; Manby, F. R. Polaritonic coupled-cluster theory. *Phys. Rev. Research* **2020**, *2*, 023262.
- (50) Flick, J.; Narang, P. Cavity-Correlated Electron-Nuclear Dynamics from First Principles. *Phys. Rev. Lett.* **2018**, *121*, 113002.
- (51) Schäfer, C.; Buchholz, F.; Penz, M.; Ruggenthaler, M.; Rubio, A. Making ab initio QED functional(s): Nonperturbative and photon-free effective frameworks for strong light-matter coupling. *Proc. Natl. Acad. Sci.* **2021**, *118*, e2110464118.
- (52) Flick, J. Simple Exchange-Correlation Energy Functionals for Strongly Coupled Light-Matter Systems Based on the Fluctuation-Dissipation Theorem. *Phys. Rev. Lett.* **2022**, *129*, 143201.
- (53) Metropolis, N.; Ulam, S. The Monte Carlo Method. *Journal of the American Statistical Association* **1949**, *44*, 335–341.
- (54) Foulkes, W. M. C.; Mitas, L.; Needs, R. J.; Rajagopal, G. Quantum Monte Carlo simulations of solids. *Rev. Mod. Phys.* **2001**, *73*, 33–83.
- (55) Thijssen, J. *Computational Physics*; Cambridge University Press, 2007.
- (56) Martin, R. M.; Reining, L.; Ceperley, D. M. *Interacting Electrons*; Cambridge University Press, 2016.
- (57) Johansson, J. R.; Nation, P. D.; Nori, F. QuTiP: An open-source Python framework for the dynamics of open quantum systems. *Computer Physics Communications* **2012**, *183*, 1760–1772.
- (58) Johansson, J. R.; Nation, P. D.; Nori, F. QuTiP 2: A Python framework for the dynamics of open quantum systems. *Computer Physics Communications* **2013**, *184*, 1234–1240.
- (59) Micca Longo, G.; Coppola, C. M.; Giordano, D.; Longo, S. The unbiased diffusion Monte Carlo: a versatile tool for two-electron systems confined in different geometries. *Eur. Phys. J. D* **2021**, *75*, 83.
- (60) Umrigar, C. J.; Nightingale, M. P.; Runge, K. J. A diffusion Monte Carlo algorithm with very small time-step errors. *The Journal of Chemical Physics* **1993**, *99*, 2865–2890.
- (61) Assaraf, R.; Caffarel, M.; Khelif, A. Diffusion Monte Carlo methods with a fixed number of walkers. *Phys. Rev. E* **2000**, *61*, 4566–4575.
- (62) Trotter, H. F. On the Product of Semi-Groups of Operators. *Proceedings of the American Mathematical Society* **1959**, *10*, 545–551.

- (63) Suzuki, M. Fractal decomposition of exponential operators with applications to many-body theories and Monte Carlo simulations. *Physics Letters A* **1990**, *146*, 319–323.
- (64) Sun, Q.; Berkelbach, T. C.; Blunt, N. S.; Booth, G. H.; Guo, S.; Li, Z.; Liu, J.; McClain, J. D.; Sayfutyarova, E. R.; Sharma, S.; Wouters, S.; Chan, G. K.-L. PySCF: the Python-based simulations of chemistry framework. *WIREs Computational Molecular Science* **2018**, *8*, e1340.
- (65) Sun, Q. et al. Recent developments in the PySCF program package. *The Journal of Chemical Physics* **2020**, *153*, 024109.
- (66) White, A. F.; Gao, Y.; Minnich, A. J.; Chan, G. K.-L. A coupled cluster framework for electrons and phonons. *The Journal of Chemical Physics* **2020**, *153*, 224112.
- (67) White, A. F.; Gao, Y.; Minnich, A. J.; Chan, G. K.-L. A coupled cluster framework for electrons and phonons. *J. Chem. Phys.* **2020**, *153*, 224112.
- (68) Mandal, A.; Vega, S. M.; Huo, P. Polarized Fock States and the Dynamical Casimir Effect in Molecular Cavity Quantum Electrodynamics. *J. Phys. Chem. Lett.* **2020**, *11*, 9215–9223.
- (69) Philbin, T. G. Generalized coherent states. *Amer. J. Phys.* **2014**, *82*, 742–748.
- (70) Tretiak, S.; Mukamel, S. Density Matrix Analysis and Simulation of Electronic Excitations in Conjugated and Aggregated Molecules. *Chem. Rev.* **2002**, *102*, 3171–3212.
- (71) Weight, B. M.; Gifford, B. J.; Tretiak, S.; Kilina, S. Interplay between Electrostatic Properties of Molecular Adducts and Their Positions at Carbon Nanotubes. *J. Phys. Chem. C* **2021**, *125*, 4785–4793.
- (72) Kilina, S.; Batista, E. R.; Yang, P.; Tretiak, S.; Saxena, A.; Martin, R. L.; Smith, D. L. Electronic Structure of Self-Assembled Amorphous Polyfluorenes. *ACS Nano* **2008**, *2*, 1381–1388.
- (73) Weight, B. M.; Zheng, M.; Tretiak, S. Signatures of Chemical Dopants in Simulated Resonance Raman Spectroscopy of Carbon Nanotubes. *J. Phys. Chem. Lett.* **2023**, *14*, 1182–1191.
- (74) Zheng, Y.; Weight, B. M.; Jones, A. C.; Chandrasekaran, V.; Gifford, B. J.; Tretiak, S.; Doorn, S. K.; Htoon, H. Photoluminescence Dynamics Defined by Exciton Trapping Potential of Coupled Defect States in DNA-Functionalized Carbon Nanotubes. *ACS Nano* **2021**, *15*, 923–933.
- (75) Wegner, F. Inverse Participation Ratio in 2 + e Dimensions. *Z. Physik B Cond. Mat.* **1980**, *36*, 209–214.
- (76) Murphy, N. C.; Wortis, R.; Atkinson, W. A. Generalized Inverse Participation Ratio as a Possible Measure of Localization for Interacting Systems. *Phys. Rev. B* **2011**, *83*.
- (77) Hu, D.; Huo, P. Ab Initio Molecular Cavity Quantum Electrodynamics Simulations Using Machine Learning Models. *J. Chem. Theory Comput.* **2023**, *19*, 2353–2368.
- (78) Kulahlioglu, A. H.; Dreuw, A. The Multistate Quantum Monte Carlo Algebraic Diagrammatic Construction Method. *J. Phys. Chem. A* **2023**, *127*, 2161–2175.
- (79) Umrigar, C. J.; Toulouse, J.; Filippi, C.; Sorella, S.; Hennig, R. G. Alleviation of the Fermion-Sign Problem by Optimization of Many-Body Wave Functions. *Phys. Rev. Lett.* **2007**, *98*, 110201.
- (80) Kim, J. et al. QMCPACK: an open source ab initio quantum Monte Carlo package for the electronic structure of atoms, molecules and solids. *J. Phys.: Condens. Matter* **2018**, *30*, 195901.
- (81) Liebenthal, M. D.; Vu, N.; DePrince, A. E. I. Assessing the Effects of Orbital Relaxation and the Coherent-State Transformation in Quantum Electrodynamics Density Functional and Coupled-Cluster Theories. *J. Phys. Chem. A* **2023**, *127*, 5264–5275.

Supporting Information

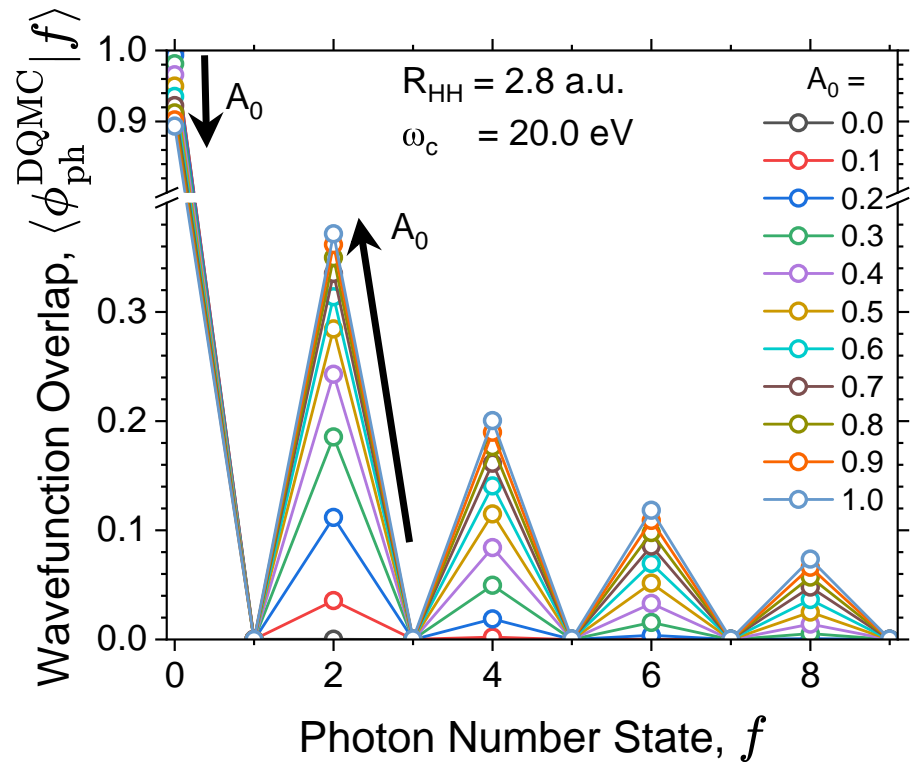


Figure S1: Photonic number state (or Fock state) expansion of the photonic DQMC wavefunction at various coupling strengths $A_0 \in (0.0, 1.0)$ a.u. for fixed cavity frequency $\omega_c = 20.0$ eV and nuclear separation length $R_{\text{HH}} = 2.8$ a.u.

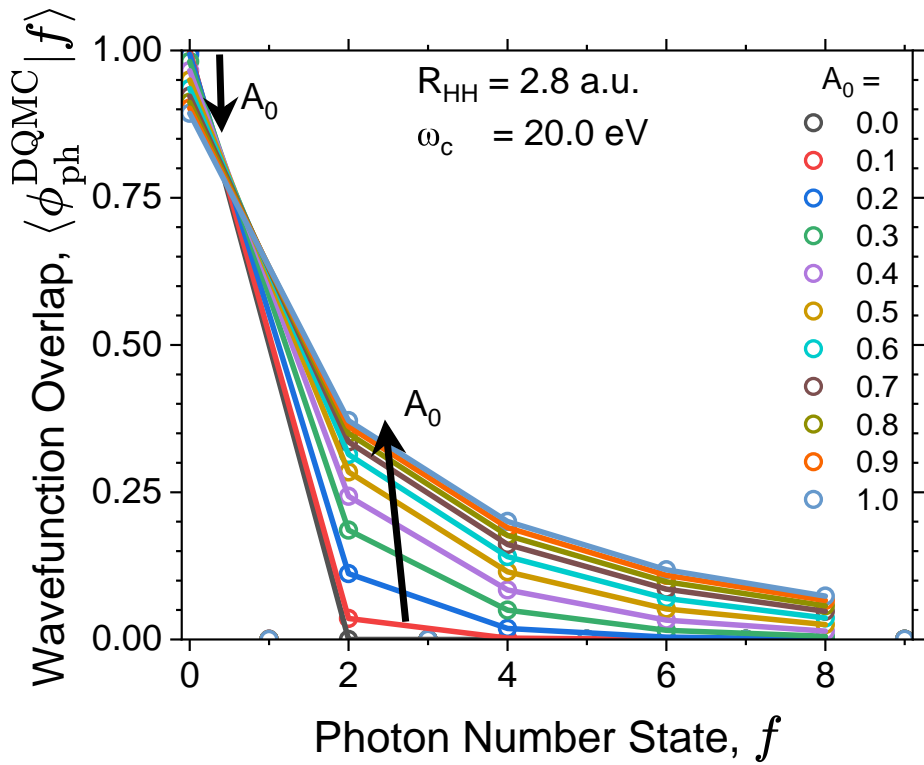


Figure S2: Photonic number state (or Fock state) expansion of the photonic DQMC wavefunction at various coupling strengths $A_0 \in (0.0, 1.0)$ a.u. for fixed cavity frequency $\omega_c = 20.0$ eV and nuclear separation length $R_{\text{HH}} = 2.8$ a.u.

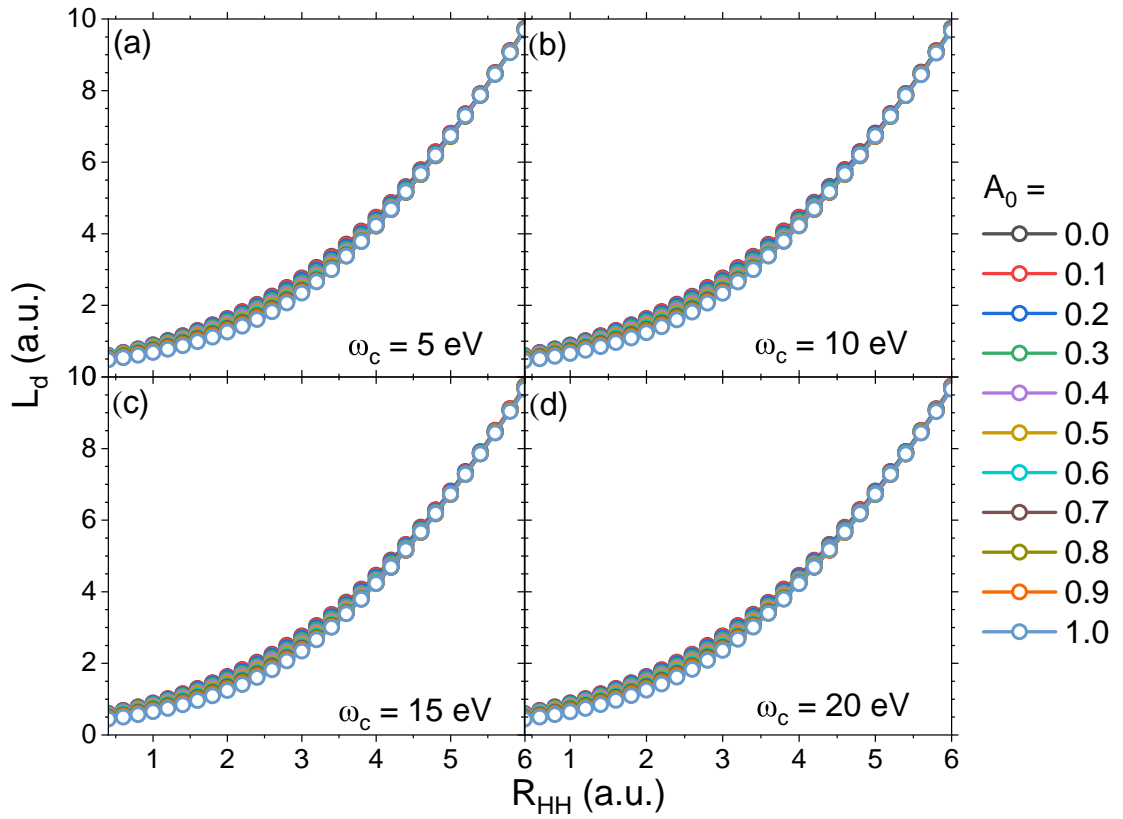


Figure S3: The wavefunction localization of the ground state H₂ dissociation, $L_d(A_0)$, at various coupling strengths A_0 (colors) for four cavity frequencies ω_c = (a) 5.0, (b) 10.0, (c) 15.0, and (d) 20.0 eV.

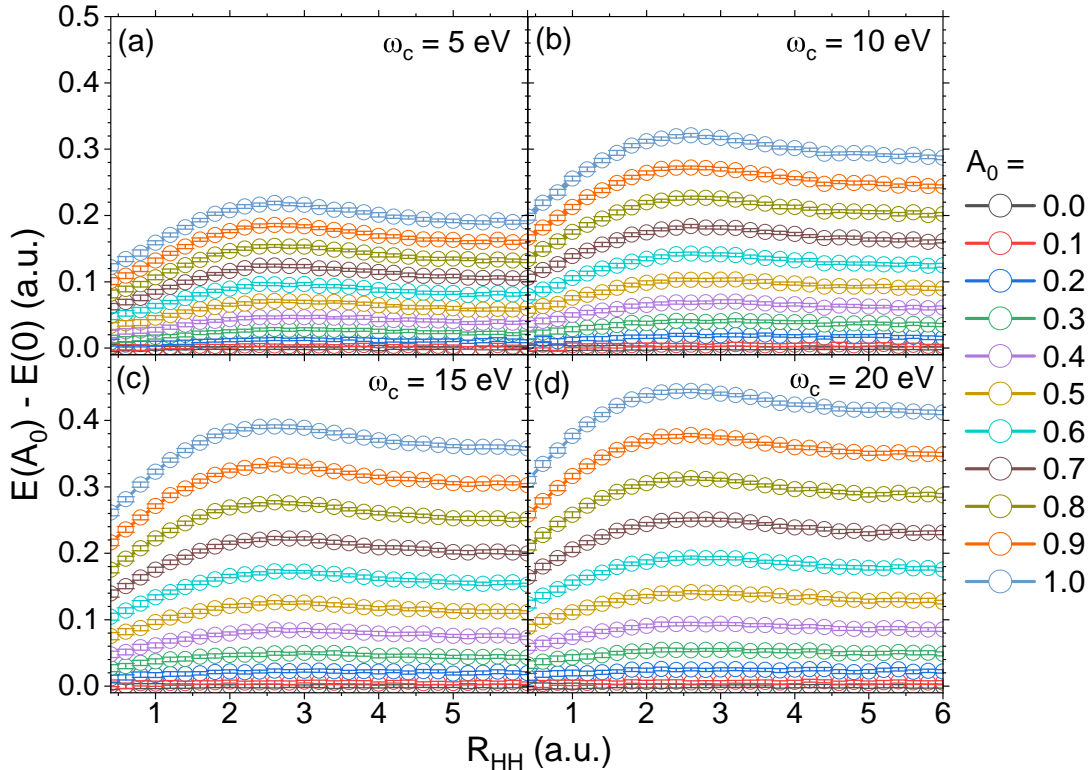


Figure S4: The energy difference of the ground state H_2 dissociation with respect to the uncoupled system (*i.e.*, $A_0 = 0.0$ a.u.) at various coupling strengths $A_0 = 0.0, 0.1, 0.2, 0.3, 0.4$, and 0.5 a.u. for four cavity frequencies $\omega_c = 5.0$ (a), 10.0 (b), 15.0 (c), and 20.0 (d) eV. The cavity polarization is parallel to the bond axis. The standard deviation of the difference of the means σ_{A-B} were calculated as $\sigma_{A-B} = \sqrt{\sigma_A^2 + \sigma_B^2}$, where σ_A and σ_B are the standard deviations of the mean for $E(A_0)$ and $E(0)$ at a fixed nuclear configuration.

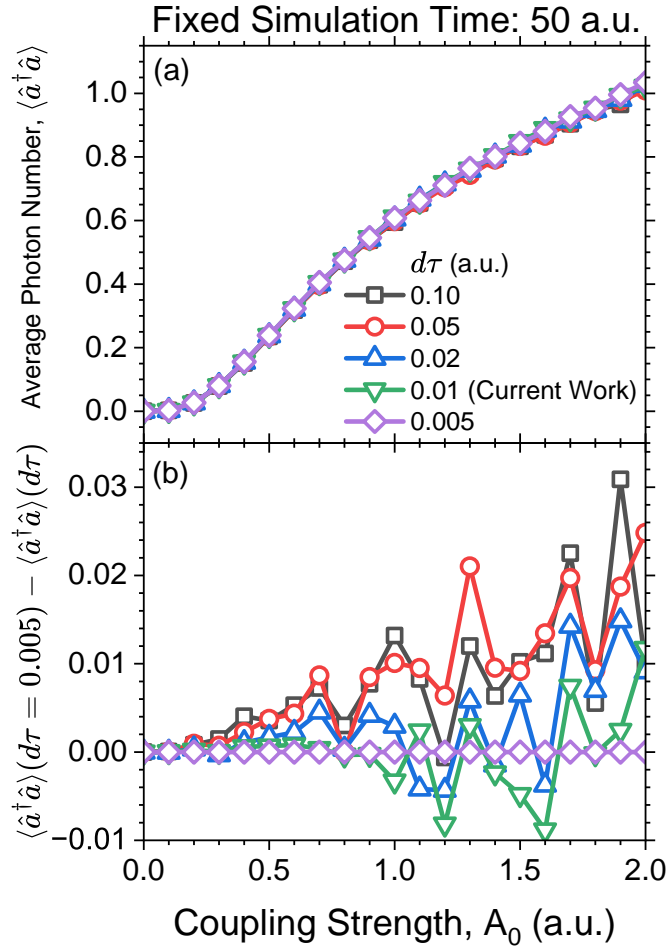


Figure S5: Convergence of the average photon number, $\langle \hat{a}^\dagger \hat{a} \rangle$ as a function of light-matter coupling strength A_0 for a fixed nuclear separation $R_{\text{HH}} = 2.8$ a.u. for a variety of simulation timesteps: $d\tau = 0.10$ (black squares), 0.05 (red circle), 0.02 (blue up triangles), 0.01 (green down triangles), and 0.005 a.u. (purple diamonds). Here, the cavity frequency is $\omega_c = 20.0$ eV, and the simulation time was kept fixed at 50.0 a.u. All data in the main text was performed with $d\tau = 0.01$ a.u.. The data presented here for $d\tau = 0.01$ a.u. is repeated from Fig. 7e in the main text and exhibits less than 1% deviation from $d\tau = 0.005$ a.u. and less than 3% deviation increasing the timestep to $d\tau = 0.10$ a.u..